Downhole Survey and Vertical Seismic Profiling at the CBRA

Shelby L. Peterie, Julian Ivanov, Marcus Tamburro, Richard D. Miller,
Brett Wedel, Cole Bunker, and Connor Umbrell

Kansas Geological Survey
1930 Constant Avenue
Lawrence, KS 66047

Final Report to

Stephen R. Hoffine
Burns & McDonnell
9400 Ward Parkway
Kansas City, MO 64114
816-839-9526

Open-file Report 2023-64 November 2023

The Kansas Geological Survey makes no warranty or representation, either express or implied, with regard to the data, documentation, or interpretations or decisions based on the use of this data including the quality, performance, merchantability, or fitness for a particular purpose. Under no circumstances shall the Kansas Geological Survey be liable for damages of any kind, including direct, indirect, special, incidental, punitive, or consequential damages in connection with or arising out of the existence, furnishing, failure to furnish, or use of or inability to use any of the database or documentation whether as a result of contract, negligence, strict liability, or otherwise. This study was conducted in complete compliance with ASTM Guide D7128-05. All data, interpretations, and opinions expressed or implied in this report and associated study are reasonably accurate and in accordance with generally accepted scientific standards.

Downhole Survey and Vertical Seismic Profiling at the CBRA

Executive Summary

Time-lapse comparison of shear-wave velocity profiles calculated from passive seismic energy has provided insights into overburden stability over the last decade and, indirectly, void dynamics at legacy salt dissolution wells in Hutchinson, Kansas. Velocity variability at Well 2A and increased depth of investigation at Well 15B suggested dynamic changes at these wells that could be related to variations in roof rock properties. Three-component, multi-offset and azimuth vertical seismic profile (VSP) data were acquired in Wells 2A and 15B to identify reflecting interfaces and assess potential signals related to voids at these wells. Anomalous amplitude and frequency variations in reflections from top of salt and inner-salt layers were observed at Well 15B and may be the result of seismic wave propagation through a void. Additional VSPs acquired in a radial pattern around Well 15B would provide insight into the characteristics of the source of the amplitude and frequency variations observed at this well. Chaotic reflection-like events observed at Well 2A are approximately consistent with expected arrivals times for P-wave diffractions from the tops of the three voids as encountered during drilling. Cementing geophones and/or fiber optic cable in the boreholes during plugging would allow for (1) time-lapse monitoring of high-resolution velocity near the borehole will significantly reduce the large spatial averaging inherent to multichannel analysis of surface waves (MASW) while allowing for cost effective use of passive or active source types, and (2) depending on source repeatability and signal to noise ratio, possibly direct differencing to image changes related to void growth or roof configuration.

Introduction

Passive multichannel analysis of surface waves (MASW) has been used to estimate shear-wave velocity (Vs) at numerous salt dissolution wells at the Carey Boulevard Research Area (CBRA) since 2013 to monitor for changes in overburden. Time-lapse comparison of Vs profiles has provided insights into consistency of overburden stability and, indirectly, void dynamics. Well 2A consistently experienced dynamic changes in velocity, most notably in 2014. Increased depth of investigation was observed across multiple years at Well 15B and was interpreted as likely resulting from elevated velocity (increased stress on rocks) at depth. These observations suggest dynamic changes at these wells that could be related to variations in roof rock properties.

To directly investigate the apparent time-lapse variability at Wells 15B and 2A, these wells were redrilled in late 2022. Due to challenges redrilling the original casing, Well 15B was drilled 8 feet (ft) east of the original well. Gamma ray logging was used to locate the top of the salt and identify voids within the salt, and sonar was used to map the voids in Well 2A. The top of salt was identified at 412 ft in both wells. In Well 15B, no void had been encountered in the salt down to a depth of 451 ft, where the drilling was terminated; however, a caliper log measuring the width of the new 15B borehole located a small void from 115-128 ft. In Well 2A, three voids were penetrated in the salt at depths of 414-450, 470-529, and 627-706 ft.

Vertical seismic profiling (VSP) is a downhole technique used for determining compressional wave (P-wave) and shear wave (S-wave) velocities and mapping reflecting interfaces and geologic structures in close proximity to a borehole (Hardage, 1985; Stewart and DiSiena, 1989). For a traditional VSP, the source is located near the borehole and provides seismic properties and imaging very near to the well. For an offset VSP, the source is located some distance from the borehole to investigate the subsurface away from the well, generally a distance less than the depth of the sensors. Three-component (3-C) multi-offset VSP data were acquired in Wells 2A and 15B to identify reflecting interfaces and assess anomalous signal that may be related to voids associated with these wells.

Acquisition and Processing

A downhole survey designed for velocity analysis and test data for evaluating the potential of VSP were collected at Well 15B on January 24, 2023 (Figure 1). The vertical seismic source was an accelerated weight drop located 20 ft north of Well 15B. The downhole receiver was a three-component (3-C) Geostuff BHG-2 geophone with steel band clamping mechanism. The natural frequency of the sensors is 10 hertz (Hz). Receiver stations were located in the borehole from 10-400 ft below ground surface at 10 ft intervals. Three consecutive shots were recorded independently and vertically stacked during processing to improve the signal-to-noise ratio. This procedure was then repeated using an IVI Minivib I in a horizontal configuration with shear plate. The sweep was a 5 second (s) linear upsweep from 10 to 150 Hz with 1 s and 0.5 s cosine tapers on the low and high ends, respectively.

Abbreviated offset VSPs were collected at source stations located 50 ft north and 200 ft west of Well 15B using a sledgehammer, plate, and shear block in addition to the weight drop and Minivib. The primary purpose of these test shots was to assess signal from different sources and offsets, determine the required number of shots for sufficient signal to noise ratio (S/N), and for preliminary evaluation of reflections at and below the top of salt.

During a second trip to the site on February 27-28, 2023, offset VSP data were collected at Wells 2A and 15B (Figure 1). Based on observations from the January survey and in-house testing, multipurpose rubber coating was applied to the exterior housing of the downhole tool and weather stripping was applied to the band to improve coupling and reduce mechanical oscillations. The source was a 16 lb sledgehammer with steel plate and shear block oriented in both longitudinal and transverse directions relative to each well. Source locations at Well 15B were 50 ft and 180 ft in the direction of Well 11B (South), and 50 and 200 ft in the direction of Well 10B ("West"). Source locations at Well 2A were 50 ft and 200 ft west. Multiple shots (3 to 6, depending on depth) were recorded independently and vertically stacked during processing to improve the S/N. Both the 50 ft and 180-200 ft offsets were acquired at each receiver depth for each azimuth prior to unlocking the tool and changing depths. An abbreviated survey was performed 200 ft south of the grain elevators; however, the survey was terminated after only 9 receiver depths due to poor data quality recorded within the zone of poor cementation (as evidenced by the cement bond log). No improvement in signal was observed regardless of variations in acquisition approach.

Figure 1. Layout of VSP surveys relative to wells 2A and 15B.

Processing and Results

Velocity Estimation

Data from 20 ft north of Well 15B were used to calculate average and interval P-wave (Vp) and S-wave velocity (Vs). Shear records from the vibroseis source were cross-correlated with a synthetic sweep during processing, collapsing the sweep signal to a Klauder wavelet. First arrivals were picked on the compressional records as first breaks of the causal, minimum-phase impulsive wavelets and as the central peak on the noncausal, zero-phase Klauder wavelets on the shear records. Average and interval velocities were calculated using picked arrival times and path length from the source to receiver (Figure 2).

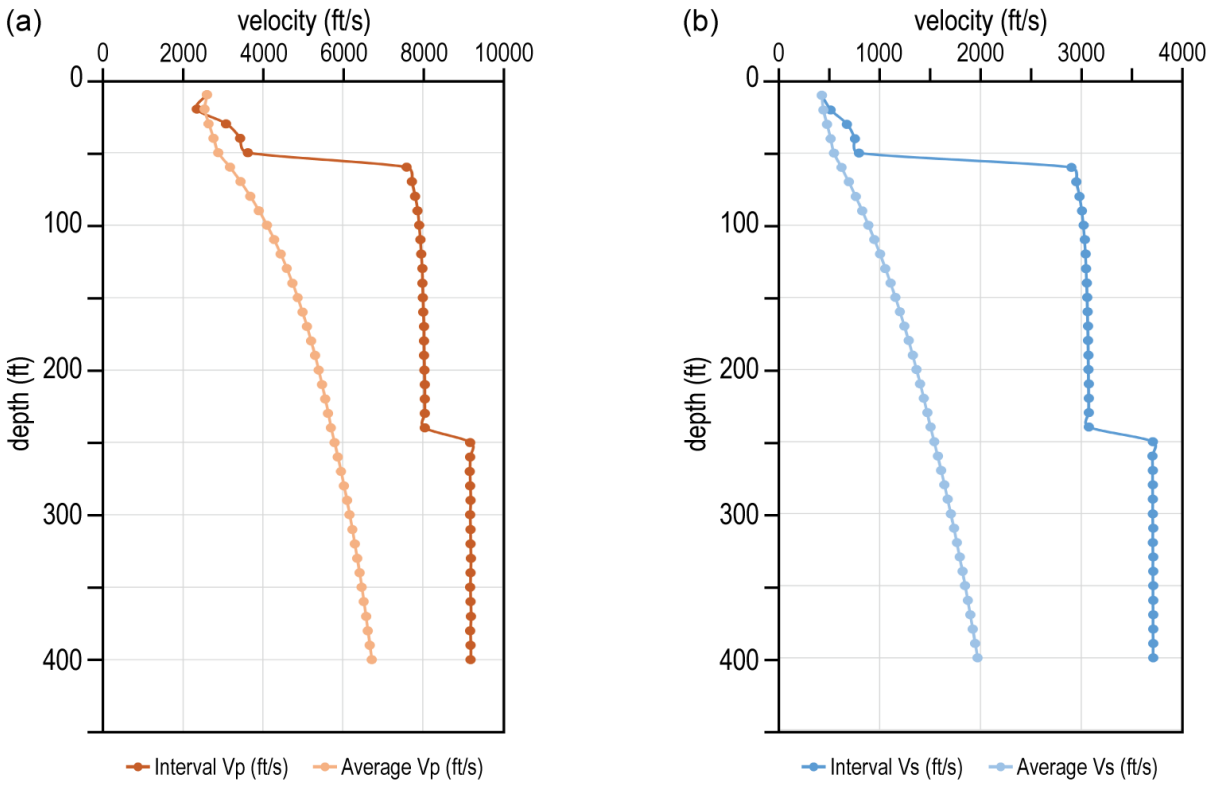

Figure 2. Average and interval (*a*) P-wave, and (*b*) S-wave velocities at well 15B.

Offset VSPs

Data from 50 ft and 180-200 ft source locations at Wells 15B and 2A were used for offset VSPs. Prior to imaging, horizontal traces were numerically rotated to the longitudinal and transverse orientations relative to the direction of the source (following the method outlined by DiSiena et al., 1984). Numerical rotation provides optimal vertically polarized shear (SV) and horizontally polarized shear (SH) waves for horizontal sources (longitudinal and transverse, respectively) (Figure 3). Vertical (P-wave), longitudinal (SV-wave), and transverse (SH-wave) records were frequency-wavenumber (*f-k*) filtered to attenuate the down-going direct waves and enhance up-going events (e.g., reflections) (Figure 4a and 4b). Static corrections based on picked first arrival times were applied to flatten reflections (Figure 4c). The complete set of raw records and offset VSPs for Wells 15B and 2A are located in the Appendix.

Discussion

The S/N is low on shallow traces (receiver location near top of hole) of all records due to poor coupling between the casing and unconsolidated sediment (Figure 4a). Strong body wave amplitudes begin at 60 ft indicating good coupling in Well 15B. This observation suggests top of bedrock between 50 and 60 ft below ground surface. Bedrock velocities are mostly consistent below 60 ft with a slight increase at approximately 250 ft, which is the expected depth of the "three finger" dolomite. The average Vs is consistent with stacking velocities from the 2008 active seismic reflection survey at the CBRA (Miller et al., 2009), and the interval bedrock velocities are similar to the interval velocities calculated using the 2008 stacking velocities. Velocity estimates from offset surveys in both Wells 15B and 2A are consistent with the downhole survey, which further supports that the interval velocities from the

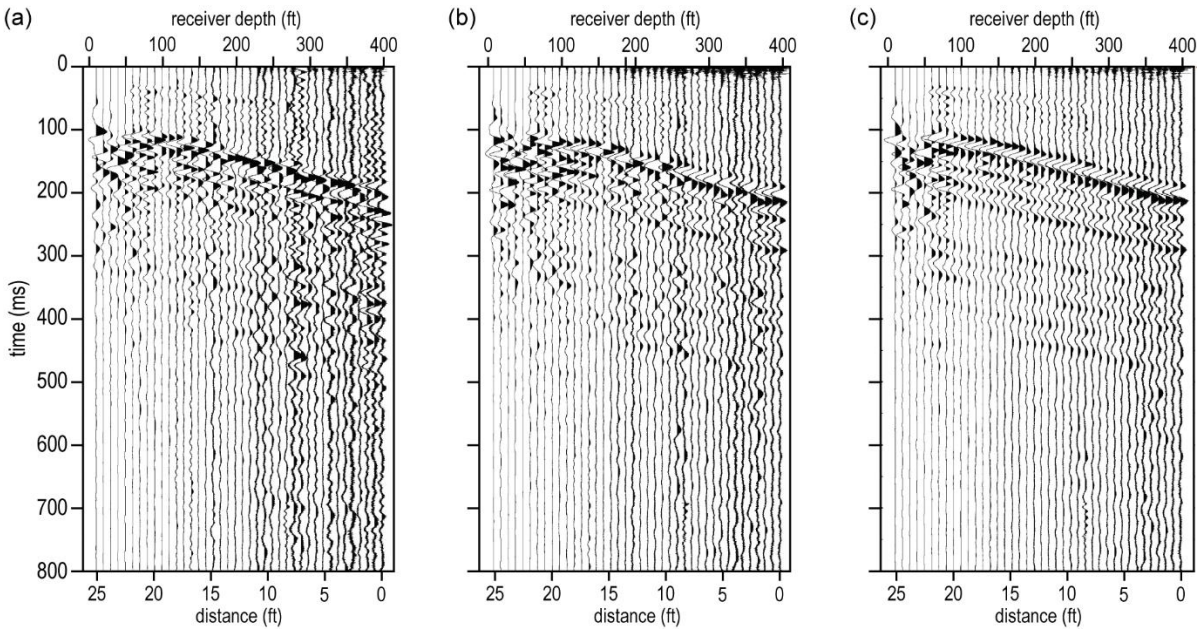

Figure 3. Traces acquired with a longitudinally oriented shear block and two perpendicular horizontal sensors (*a* and *b*) prior to numerical rotation, and (*b*) after numerical rotation. S-wave amplitudes are random prior to numerical rotation due to random orientation of the downhole tool. SV-wave amplitudes are optimized on the longitudinal traces (*b*) and minimal on the transverse traces after numerical rotation.

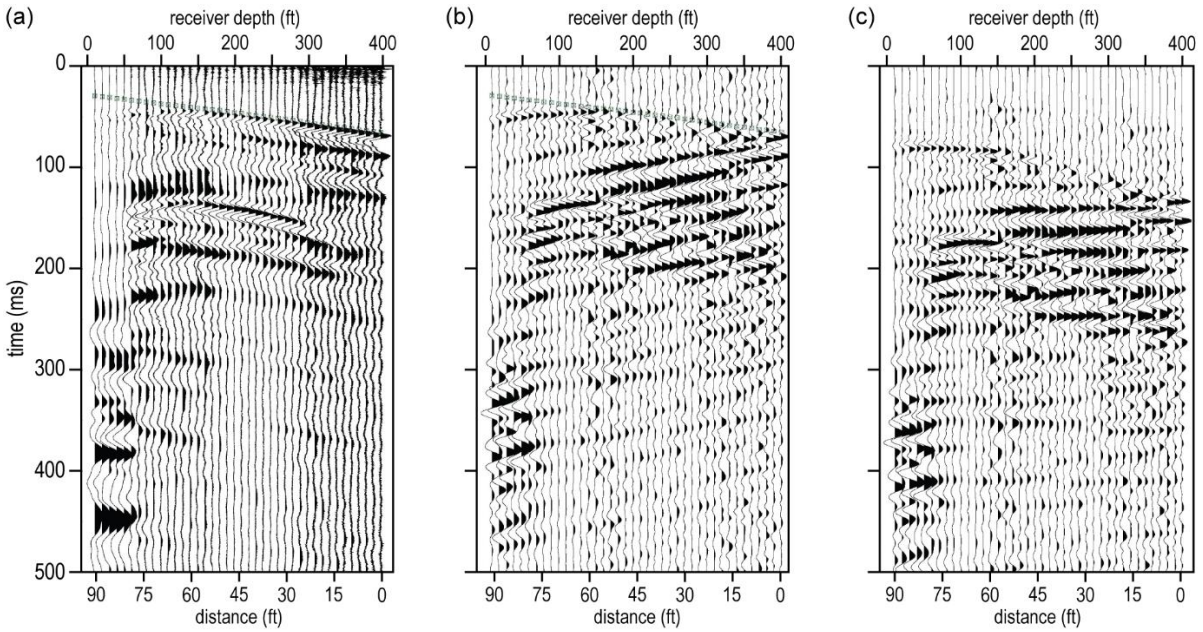

Figure 4. Vertical (P-wave) record from the source located 180 ft south of well 15B (*a*) unfiltered, (*b*) after *f-k* and bandpass filtering, and (*c*) after static corrections. Green squares in (*a*) and (*b*) represent the picked first arrival times used for static corrections to produce (*c*).

downhole survey in 15B are likely representative for this site. However, the interval bedrock Vs is much faster than Vs obtained from passive MASW surveys. This implies that Vs obtained from MASW are likely less than the true velocity.

To investigate the discrepancy between the downhole and the passive MASW bedrock velocities, synthetic seismic data were generated with the velocity model obtained from the downhole survey. The dispersion pattern on phase velocity–frequency plot of the synthetic data is nearly identical to the real passive surface wave data (Figure 5). Dispersion curves were modeled using a simplified 3-layer model based on the velocities from downhole survey (Table 1). The calculated fundamental mode dispersion curve matches the dominant trend on phase velocity–frequency plots, indicating the dominant trend is the fundamental mode. The Vs model obtained from MASW and the model obtained from the downhole survey produce nearly identical dispersion curves. This is known as non-uniqueness and is a well-recognized concern for MASW and other inversion-based methods (Sambridge, 2001; Wathelet et al., 2004; Socco et al., 2010; Foti et al., 2015). Without additional *a priori* information to constrain the inversion, both models would be equally valid potential solutions.

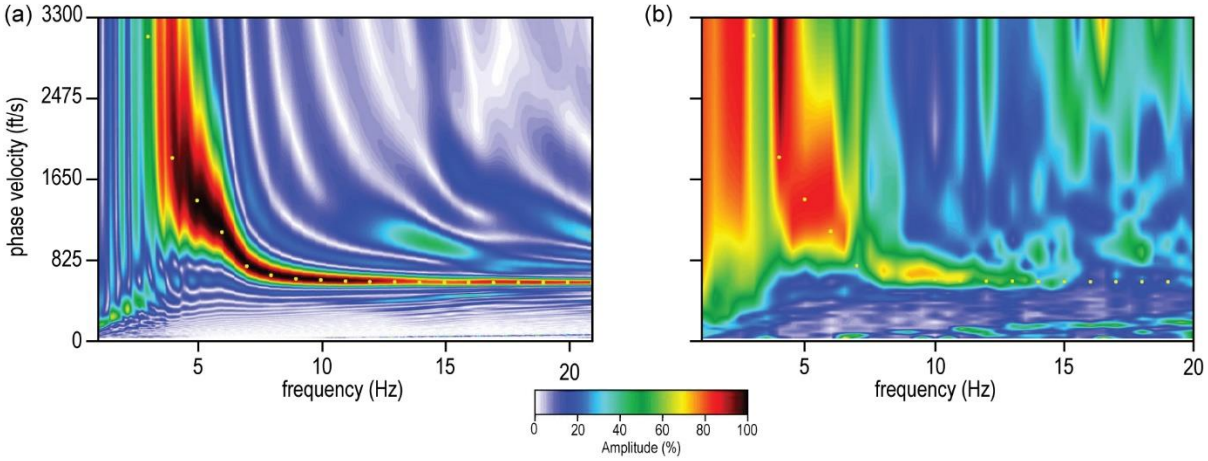

Figure 5. Dispersion curves for (*a*) the synthetic model using VSP velocities, and (*b*) 2021 passive MASW survey. Yellow dots represent the calculated fundamental mode dispersion curve for the VSP velocities.

Table 1. Simplified 3-layer model based on the velocities from downhole survey.

Layer	Thickness (ft)	Vs (ft/s)
1	50	620
2	190	3,000
3	halfspace	3,700

When generating an initial model for surface wave inversion the conventional assumption is that phase velocity is proportional to the interval velocity at 1/3 to 1/2 of the corresponding wavelength. However, in this case, the phase velocities may represent the average surface wave velocity between the surface and the depth of the corresponding wavelength. This would explain the low apparent velocities that gradually increase with depth. The effect of averaging would be minimal where velocity changes are gradational, such as sedimentary layers in the shallow subsurface—the usual target in MASW surveys. Low bedrock velocities have been noted in

other studies, and inversion results were highly sensitive to the initial model (Casto et al., 2009). For this site, absolute velocity is not necessary to assess changing stress conditions overlying salt jugs. Rather, relative velocity and temporal velocity change are key for assessing stress and changing conditions and more than sufficient for monitoring purposes.

Reflections from the top of salt and from within the salt are observed on VSPs from Well 15B. In general, reflections on P-wave VSPs have a higher S/N compared to S-wave VSPs, especially at longer offsets. P-wave reflections from the top of and within the salt are coherent and high-frequency on most traces. However, primarily at the 180 ft South source offset location, amplitude and frequency variations are observed in reflections from top of salt and inner-salt reflections on traces recorded at receiver depths between 130 ft and 320 ft (Figure 6). At receiver depths below 320 ft, the amplitude and frequency of these deeper reflections return to normal and are consistent with other receiver depths and source locations. The cause of the amplitude and frequency variations is unclear but could be the result of wave propagation through a void.

Hyperbolic events are evident on P-wave VSPs from Well 15B, particularly at the 180 ft South shot location (Figure 6b). The earliest arrival time (apex) at a receiver depth of 110-120 ft suggests the origin of this event is at this depth. A similar event, although lower in amplitude, is also observed at the 200 ft West shot location (Figure A-5a in the Appendix). Additionally, what appears to be a P-S mode-converted wave originating from the same depth is observed at the 200 ft West source location. (Similar events are also observed on records with the source 200 ft West of Well 2A, Figure A-5a). Without additional information, the origin of these events remains unclear. It is possible these are S-P mode-converted waves, and unrelated to the salt jugs. Multi-azimuth offset VSPs in a regular, radial pattern around Well 15B would provide pseudo-3D imaging to assess the origin of the hyperbolic events, mode-converted wave, and amplitude and frequency characteristics of reflections from the top of salt or within the salt.

At Well 2A, the gamma ray density log and sonar indicate three large voids from 410-450 ft, 470-530 ft, and 625-705 ft. The cement bond log suggests variable cementation for about half of the cased interval between top of bedrock and the deepest receiver station, which impacts coupling of the downhole receiver with the formation through this interval. Similar to Well 15B, S/N is lower overall on the S-wave VSPs, and relatively coherent reflections are only observed on the S-wave VSPs at the 50 ft West source location, but with no clear indications of diffractions or anomalous signal associated with the presence of the voids (Figure 7). Arrivals on the P-wave VSP at the 200 ft West source location are chaotic and challenging to interpret (Figure 8a). This is likely the result of a combination of variable cementation and scattered signal from multiple voids in the salt. Reflection-like events between 130-200 ms that are not perfectly flattened after static corrections are approximately consistent with expected arrivals times for P-wave diffractions from the tops of the three voids within the salt (Figure 8b).

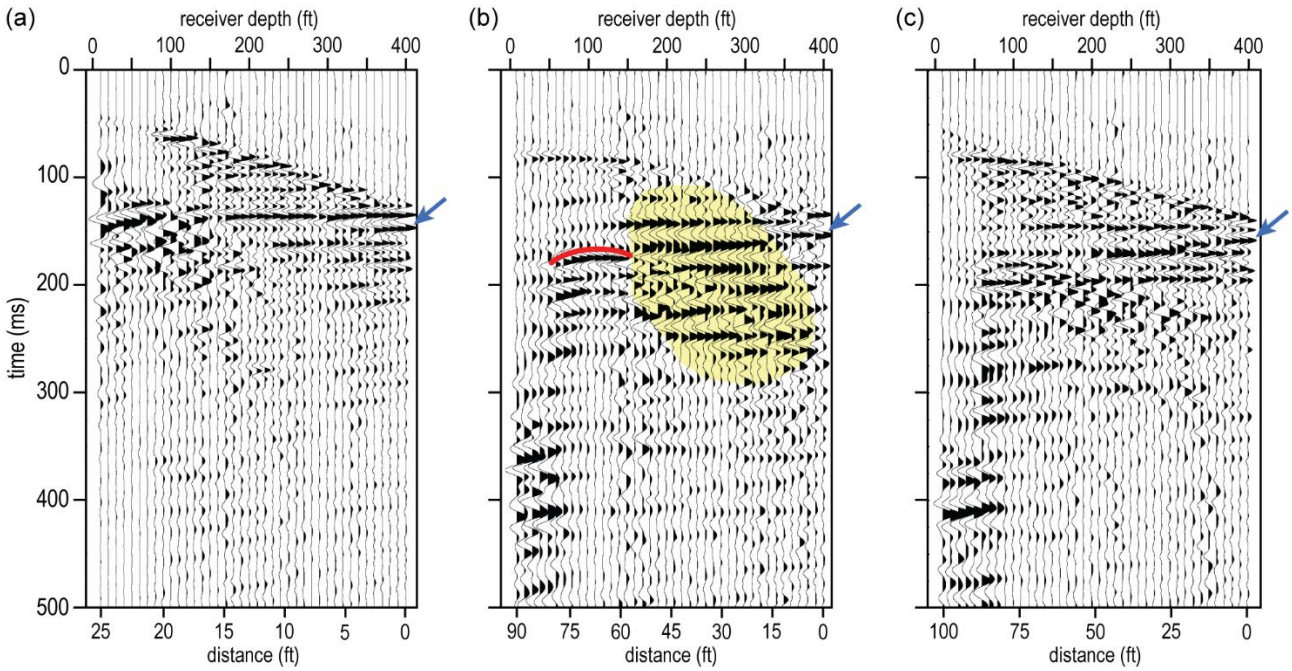

Figure 6. P-wave VSP from (*a*) 50 ft South, (*b*) 180 ft South, and (*c*) 200 ft West of well 15B. Possible P-S converted wave (red) and amplitude and phase variations (yellow) are interpreted in (*b*). Blue arrows indicate possible reflections from the top of the void.

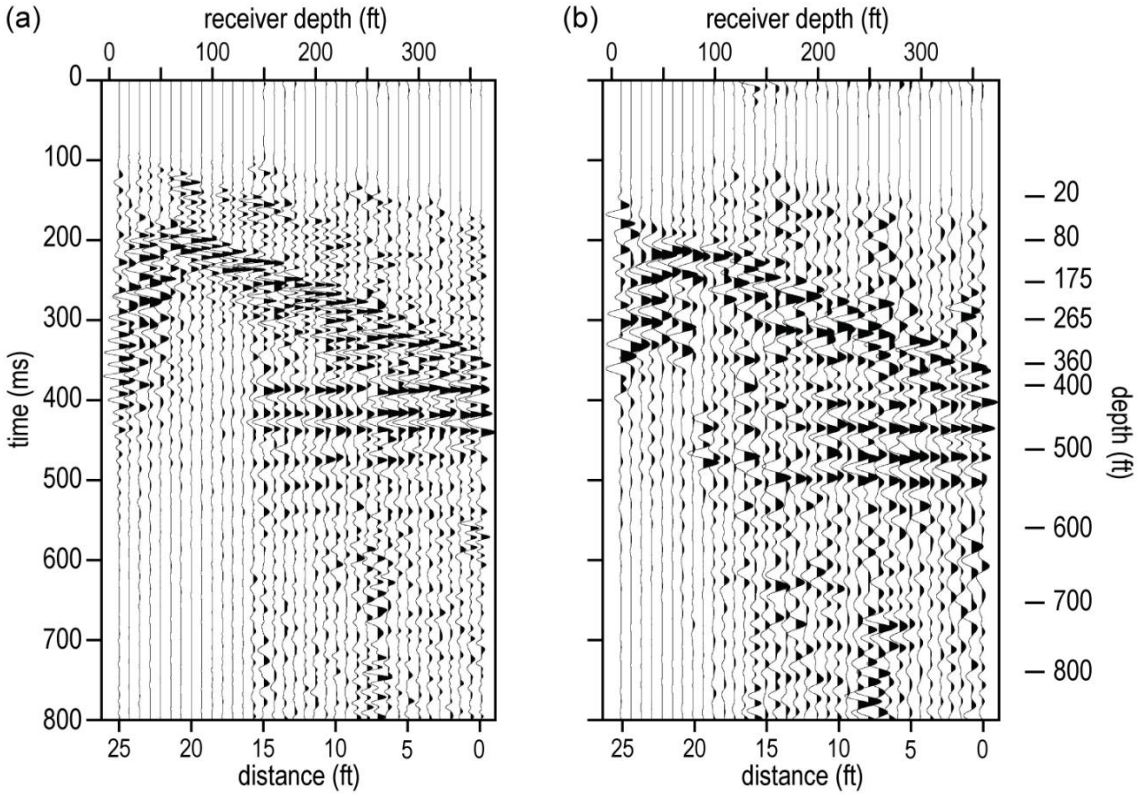

Figure 7. (*a*) Longitudinal and (*b*) transverse S-wave VSPs from 50 ft West of well 2A.

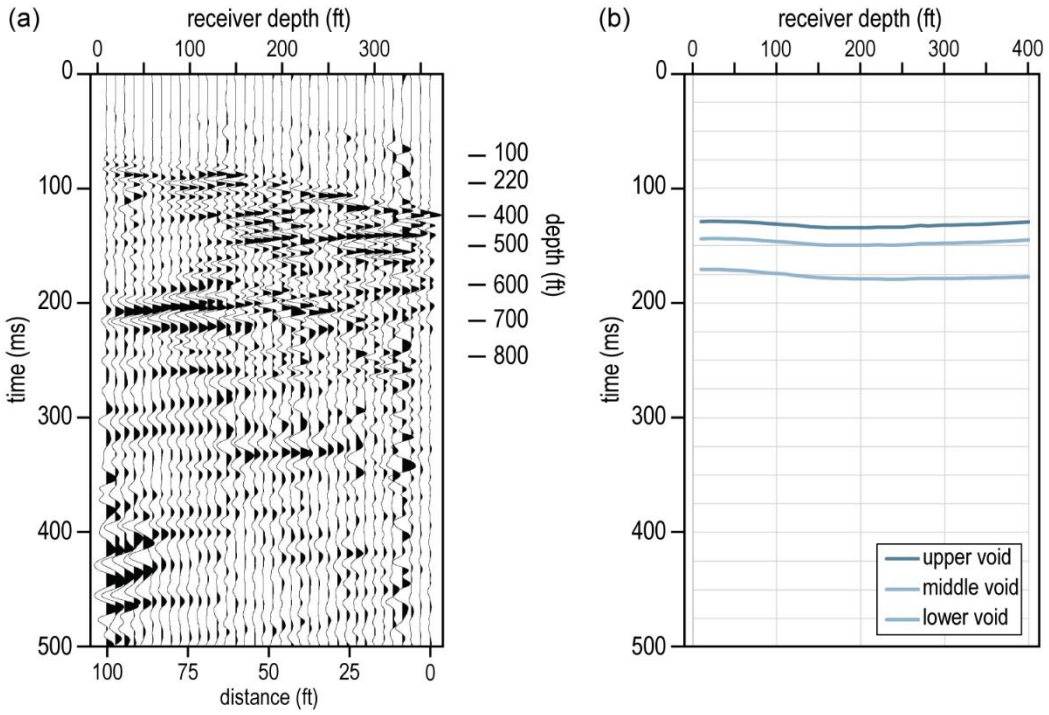

Figure 8. (*a*) P-wave VSP from 200 ft West of well 2A. (*b*) Calculated arrival times for P-wave diffractions from the top of each void centered at the well.

Conclusions and Recommendations

The downhole survey provided accurate values for absolute velocity at this site. Vs from the downhole survey at Well 15B differ from Vs obtained from passive MASW due to non-uniqueness, where different velocity models produce similar dispersion patterns and are equally valid without additional *a priori* information. Velocities on the dispersion curve appear to possibly correspond to the average velocity at the depth of the associated wavelength. Because the initial velocity model for the MASW inversion was based on the conventional assumption that the velocity corresponds to the interval velocity at a depth of half the wavelength, MASW produced a velocity model with more gradational changes and overall lower velocities than the Vs borehole survey. The downhole survey indicates that the bedrock interface has a much sharper velocity gradient and overall faster velocities. Although the absolute velocity is faster than predicted by MASW, relative velocity and time-lapse velocity changes are used to assess stress conditions above the salt jugs. Therefore, previous relative velocity changes observed in MASW results at the CRBA are likely indicative of true velocity (and, thus, stress) changes. We recommend additional testing and modeling to assess calibration of MASW with an initial model based on borehole velocities to more accurately represent material properties, however, previous analysis accurately defines changes in the subsurface and perfectly suited for this monitoring application

Anomalous amplitude and frequency variations in top of salt and inner-salt reflections were observed at Well 15B. These anomalous characteristics were notably more prominent at the 180 ft South source location, indicating spatial variability and suggesting the cause of these variations are not related to the well itself. The cause is unclear but because wave propagation

through/around a void can result in changes in frequency and amplitude, these observations may suggest a void offset from the borehole in the direction of Well 11B. Multiple VSPs collected in a radial pattern around Well 15B would provide pseudo-3D imaging with higher spatial coverage and insight into the source of the anomalous signal.

Hyperbolic arrival patterns on the P-wave VSP from Well 2A are likely P-wave diffractions from the three large voids mapped via sonar within the salt. Interaction of the stress fields from these stacked voids could result in complex variations in bedrock stress and therefore shear-wave velocity over time. The notable velocity variations consistently observed using MASW at this well suggested void dynamics, which was unexpected based on the (likely incomplete) tonnage records originally attributed to this well. The presence of three large voids supports the use of time-lapse MASW as a tool for assessing void stability.

Permanent installation of geophone arrays and/or fiber optic cable during plugging could be considerable value added for relatively little additional cost. This would provide the opportunity for active or passive time-lapse monitoring at these wells, potentially addressing both velocity and imaging needs. Time-lapse velocity from downhole surveys would be high-resolution and less prone to uncertainties inherent to passive sources used for the MASW surveys at this site. Depending on source repeatability, time-lapse VSPs would likely allow for direct differencing to image subtle changes related to void growth or roof configuration changes.

References

Casto, D.W., B. Luke, C. Calderon-Macias, and R. Kaufmann, 2009, Interpreting Surface-Wave Data for a Site with Shallow Bedrock: Journal of Environmental Engineering Geophysics, 14, 3, 115-127, http://dx.doi.org/10.2113/JEEG14.3.116.

Foti, S., G.L. Carlo, G.J. Rix, and C. Strobbia, 2015, Surface Wave Methods for Near-Surface Site Characterization: CRC Press.

DiSiena, J.P., J.E. Gaiser, and D. Corrigan, 1984, Horizontal components and shear wave analysis of three component VSP data, in *Vertical Seismic Profiling, Part B: Advanced Concepts*, pp. 175-235, eds Toksoz, M.N. and R.R. Stewart, Geophysical Press, London.

Hardage, B.A., Veritical Seismic Profiling: *The Leading Edge*, 4, 11, 59-60, https://doi.org/10.1190/1.1487141.

Miller, R.D., J. Ivanov, S.D. Sloan, S.L. Walters, B. Leitner, A. Rech, B.A. Wedel, A.R. Wedel, J.M. Anderson, O.M. Metheny, and J.C. Schwarzer, 2009, Shear-wave Seismic Study above Vigindustries, Inc. Legacy Salt Jugs in Hutchinson: Kansas Geological Survey, Open-File Report 2009-3.

Sambridge, M., 2001, Finding acceptable models in nonlinear inverse problems using a neighbourhood algorithm: Inverse Problems, 17, 387, https://doi.org/10.1088/0266-5611/17/3/302.

Socco, L.V., S. Foti, and D. Boiero, 2010, Surface-wave analysis for building near-surface velocity models — Established approaches and new perspectives, 75, 75A83-75A102,

Stewart, R.R., and J.P. DiSiena, 1989, The values of VSP in interpretation: *The Leading Edge*, 8, 12, 16-23, https://doi.org/10.1190/1.1439597.

Wathelet, M., D. Jongmans, and M. Ohrnberger, 2004, Surface-wave inversion using a direct search algorithm and its application to ambient vibration measurements: Near Surface Geophysics, 2, 211-221, https://doi.org/https://doi.org/10.3997/1873-0604.2004018.

Appendix

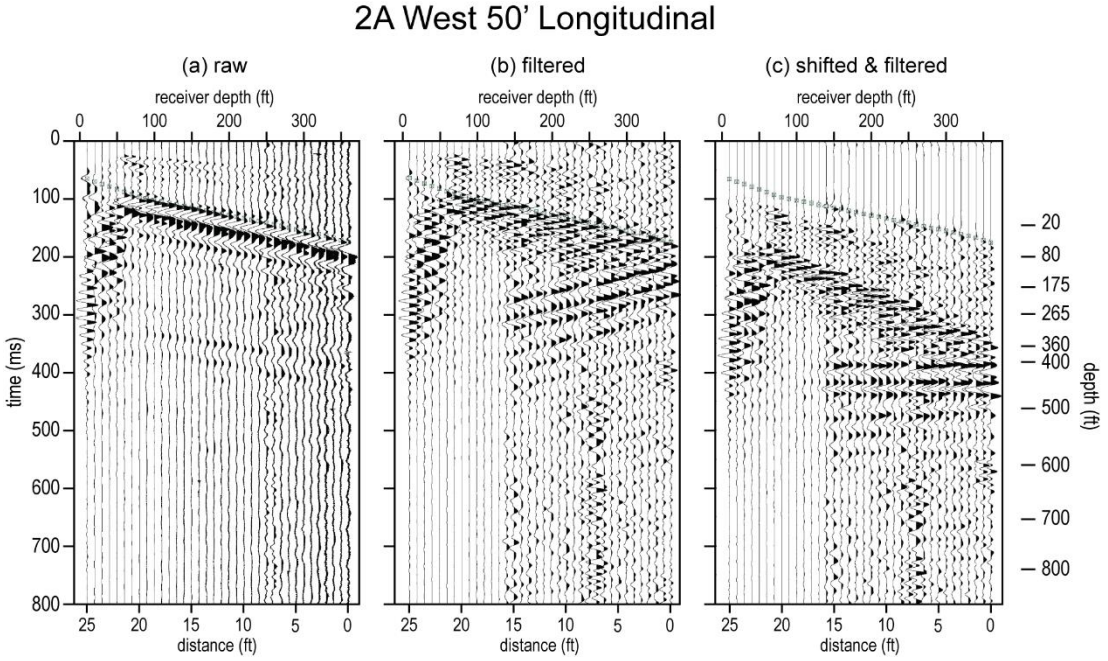

Figure A-1. Longitudinal VSP for the source station 50 ft west of Well 2A (*a*) unprocessed with picked first arrivals (green), (*b*) filtered, and (*c*) after static corrections, shifted to one-way vertically incident travel time.

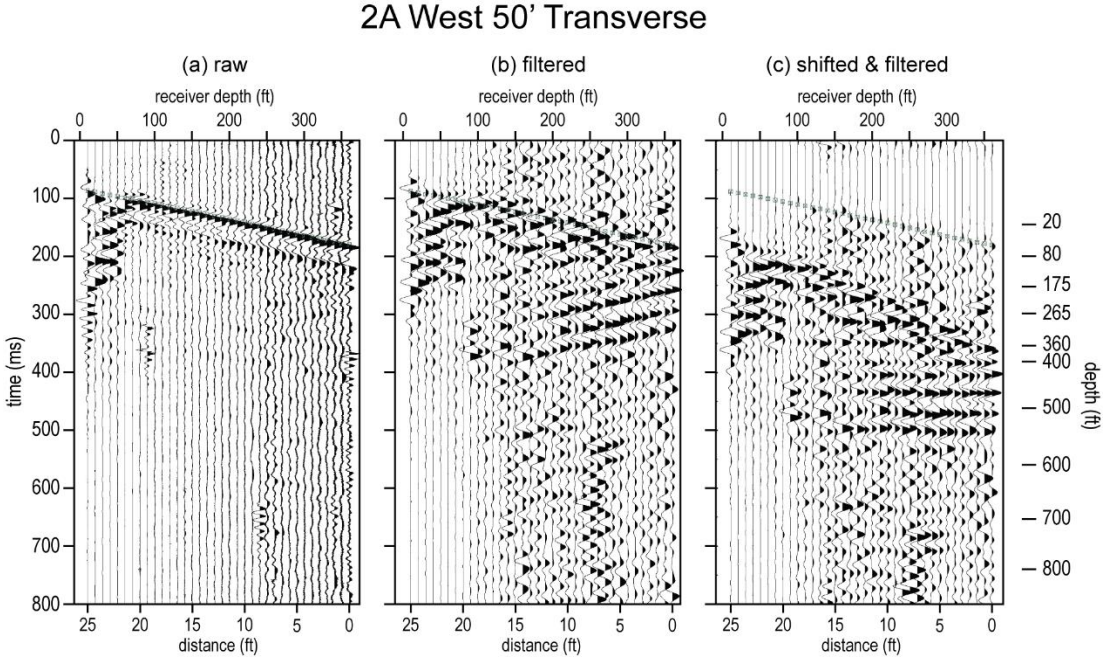

Figure A-2. Transverse VSP for the source station 50 ft west of Well 2A (*a*) unprocessed with picked first arrivals (green), (*b*) filtered, and (*c*) after static corrections, shifted to one-way vertically incident travel time.

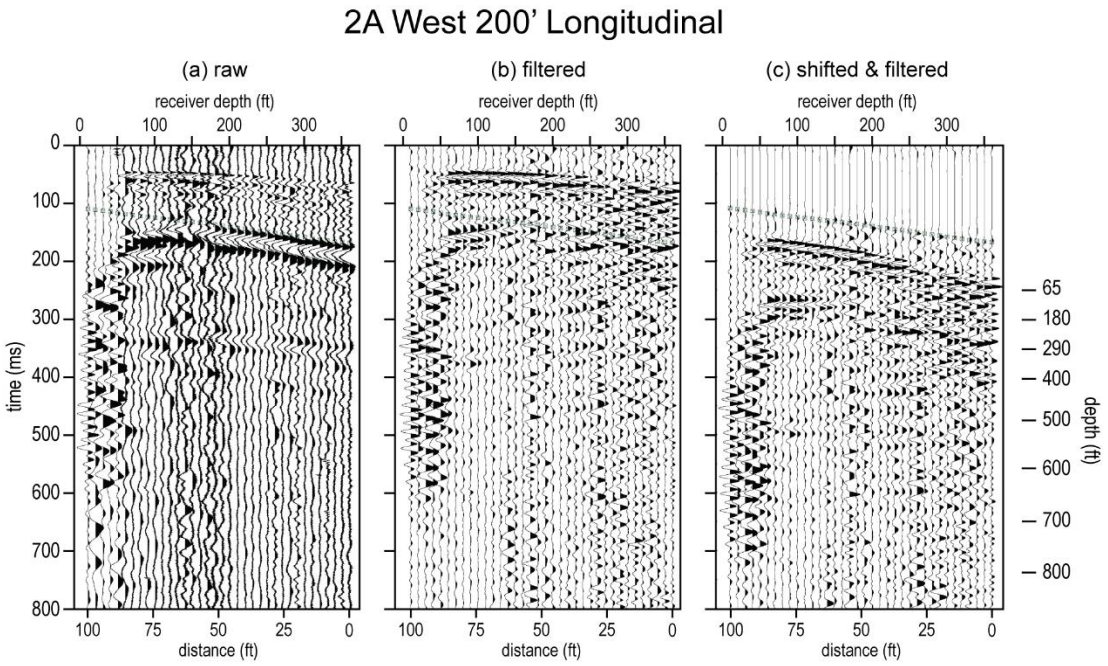

Figure A-3. Longitudinal VSP for the source station 200 ft west of Well 2A (*a*) unprocessed with picked first arrivals (green), (*b*) filtered, and (*c*) after static corrections, shifted to one-way vertically incident travel time.

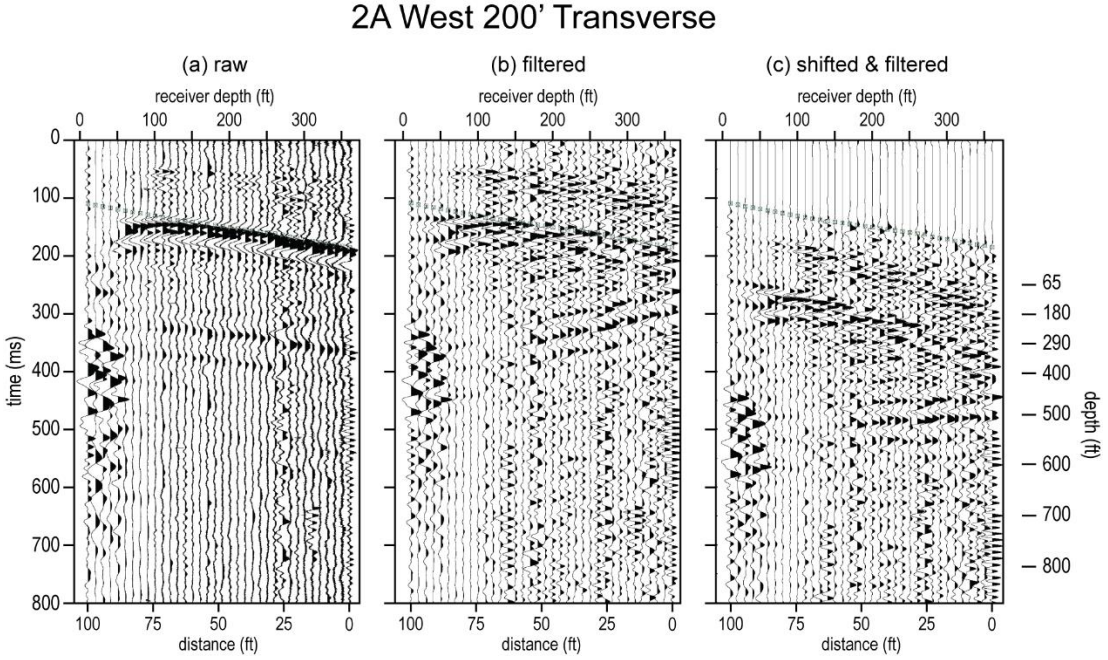

Figure A-4. Transverse VSP for the source station 200 ft west of Well 2A (*a*) unprocessed with picked first arrivals (green), (*b*) filtered, and (*c*) after static corrections, shifted to one-way vertically incident travel time.

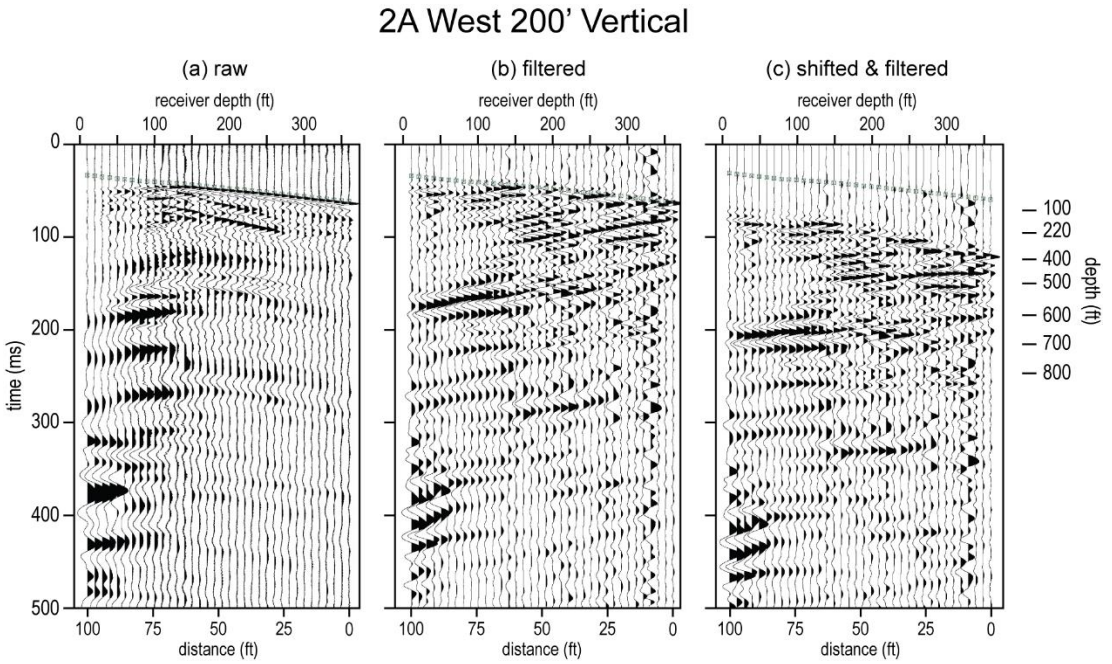

Figure A-5. Vertical VSP for the source station 200 ft west of Well 2A (*a*) unprocessed with picked first arrivals (green), (*b*) filtered, and (*c*) after static corrections, shifted to one-way vertically incident travel time.

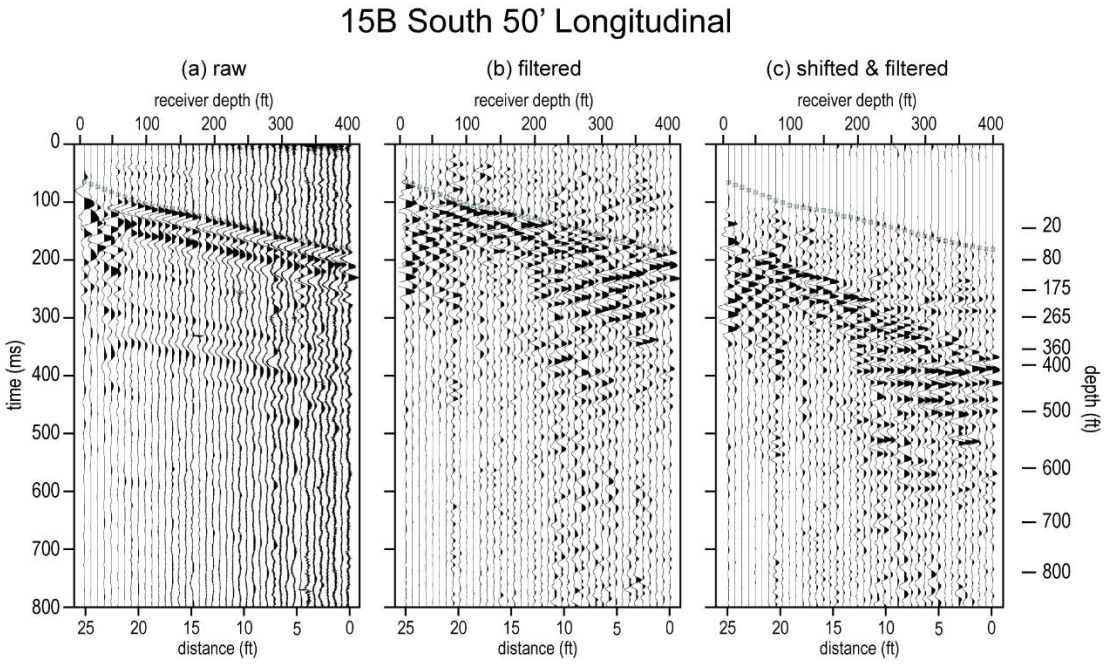

Figure A-6. Longitudinal VSP for the source station 50 ft south of Well 15B (*a*) unprocessed with picked first arrivals (green), (*b*) filtered, and (*c*) after static corrections, shifted to one-way vertically incident travel time.

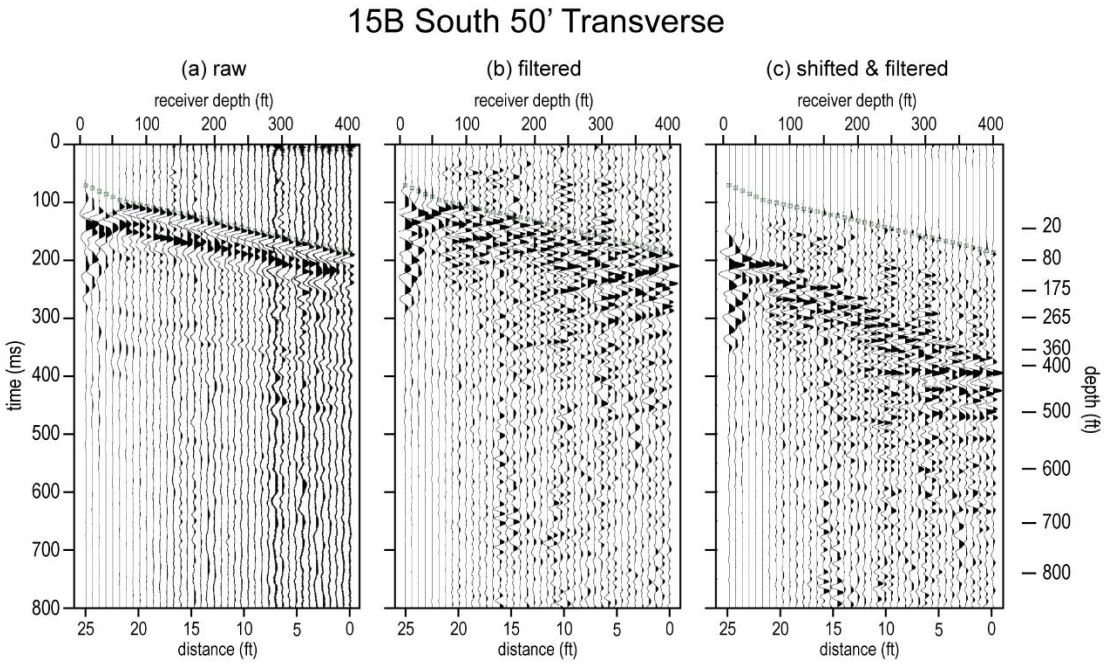

Figure A-7. Transverse VSP for the source station 50 ft south of Well 15B (*a*) unprocessed with picked first arrivals (green), (*b*) filtered, and (*c*) after static corrections, shifted to one-way vertically incident travel time.

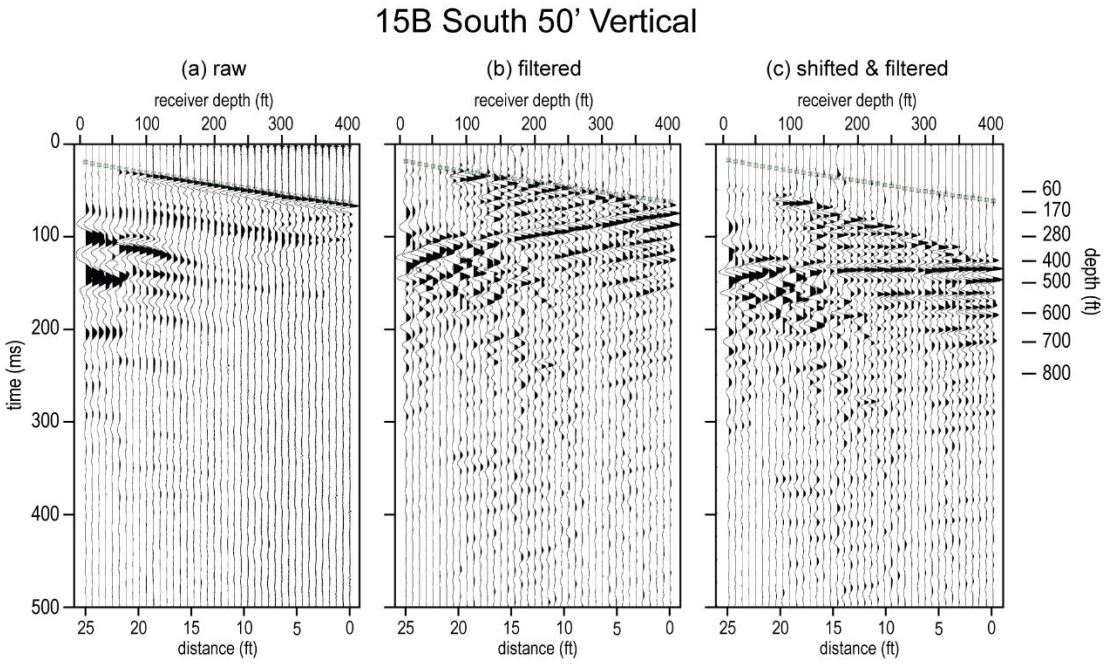

Figure A-8. Vertical VSP for the source station 50 ft south of Well 15B (*a*) unprocessed with picked first arrivals (green), (*b*) filtered, and (*c)* after static corrections, shifted to one-way vertically incident travel time.

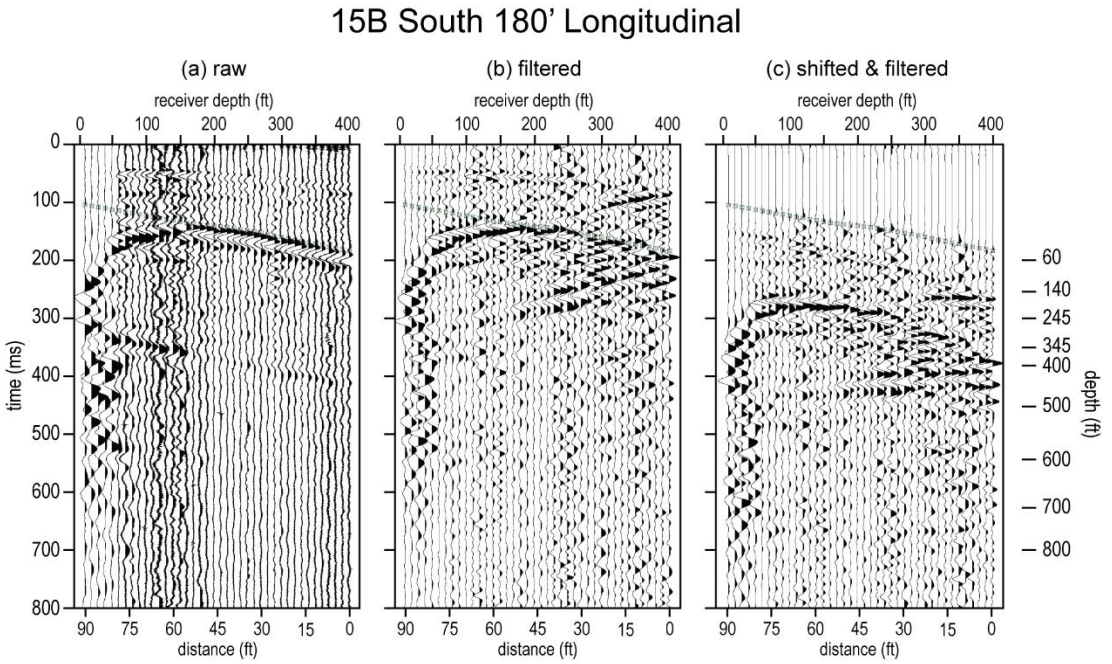

Figure A-9. Longitudinal VSP for the source station 180 ft south of Well 15B (*a*) unprocessed with picked first arrivals (green), (*b*) filtered, and (*c*) after static corrections, shifted to one-way vertically incident travel time.

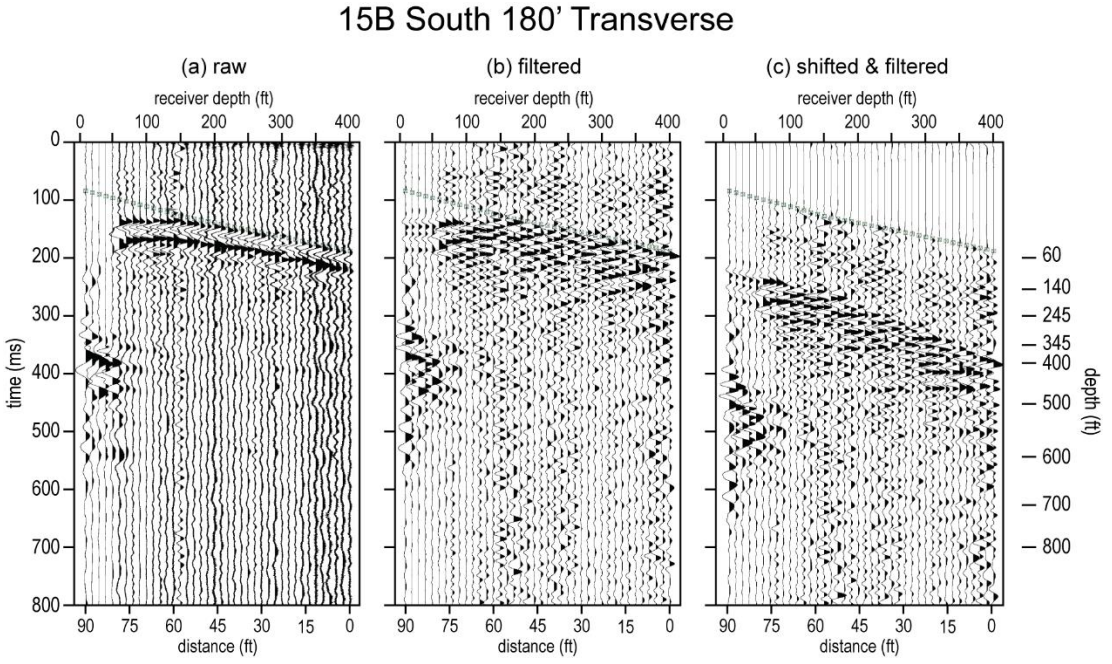

Figure A-10. Transverse VSP for the source station 180 ft south of Well 15B (*a*) unprocessed with picked first arrivals (green), (*b*) filtered, and (*c*) after static corrections, shifted to one-way vertically incident travel time.

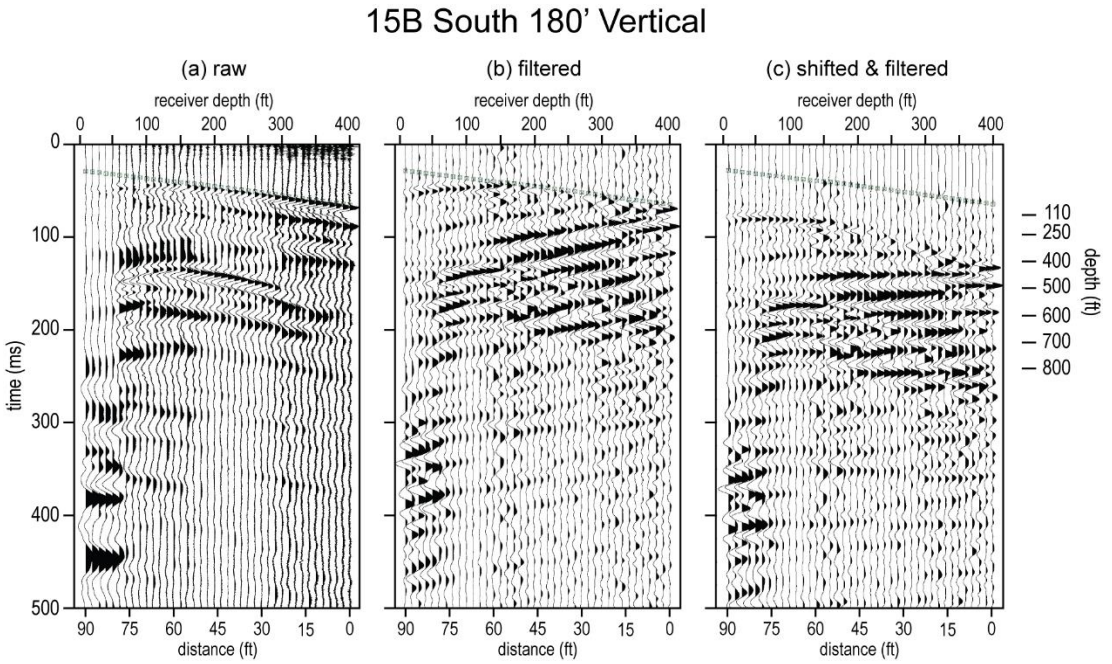

Figure A-11. Vertical VSP for the source station 180 ft south of Well 15B (*a*) unprocessed with picked first arrivals (green), (*b*) filtered, and (*c*) after static corrections, shifted to one-way vertically incident travel time.

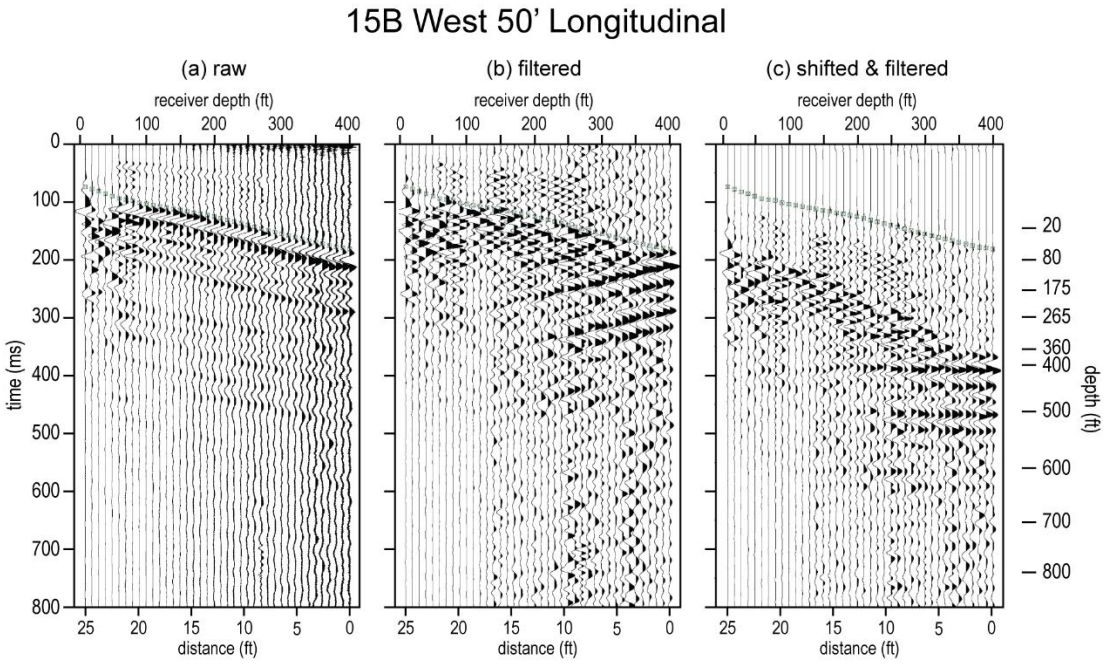

Figure A-12. Longitudinal VSP for the source station 50 ft west of Well 15B (*a*) unprocessed with picked first arrivals (green), (*b*) filtered, and (*c*) after static corrections, shifted to one-way vertically incident travel time.

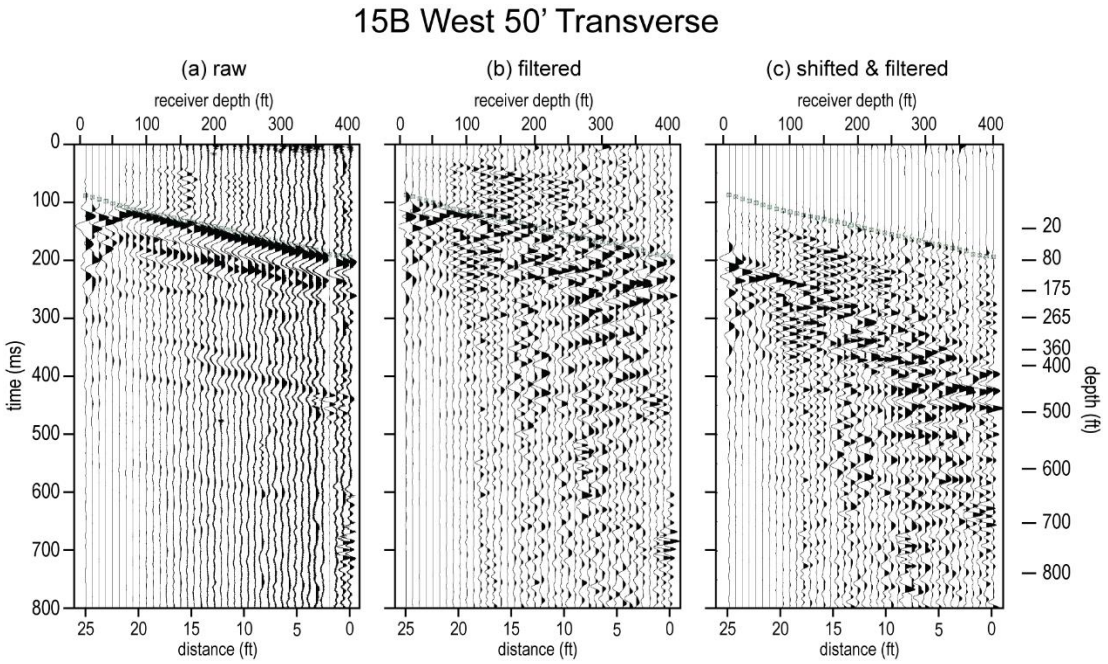

Figure A-13. Transverse VSP for the source station 50 ft west of Well 15B (*a*) unprocessed with picked first arrivals (green), (*b*) filtered, and (*c*) after static corrections, shifted to one-way vertically incident travel time.

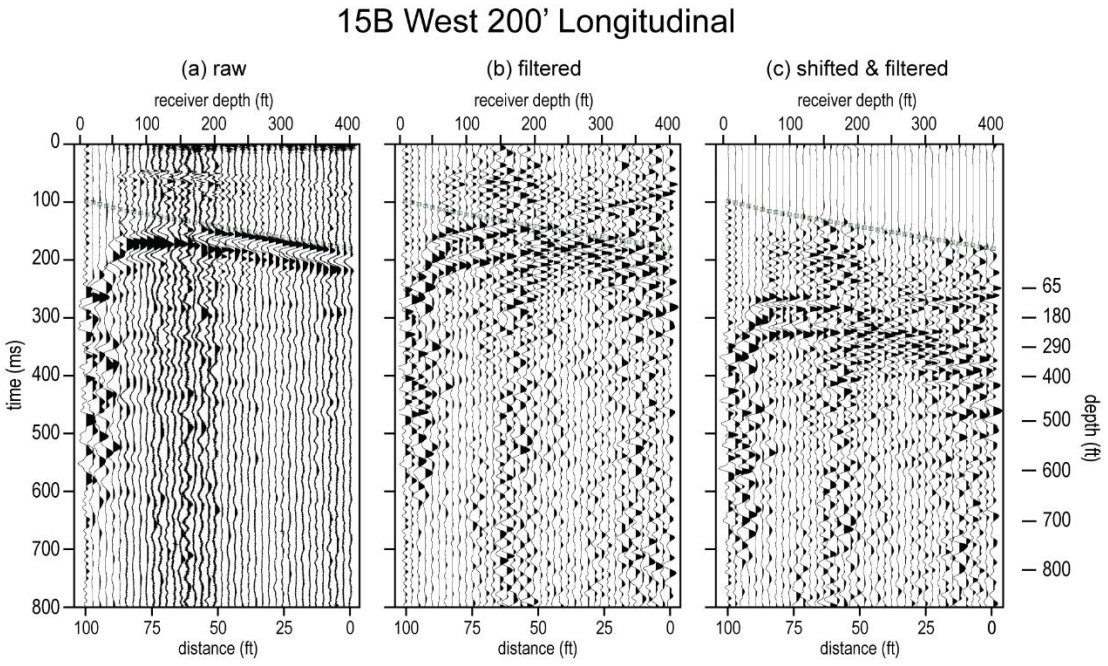

Figure A-14. Longitudinal VSP for the source station 200 ft west of Well 15B (*a*) unprocessed with picked first arrivals (green), (*b*) filtered, and (*c*) after static corrections, shifted to one-way vertically incident travel time.

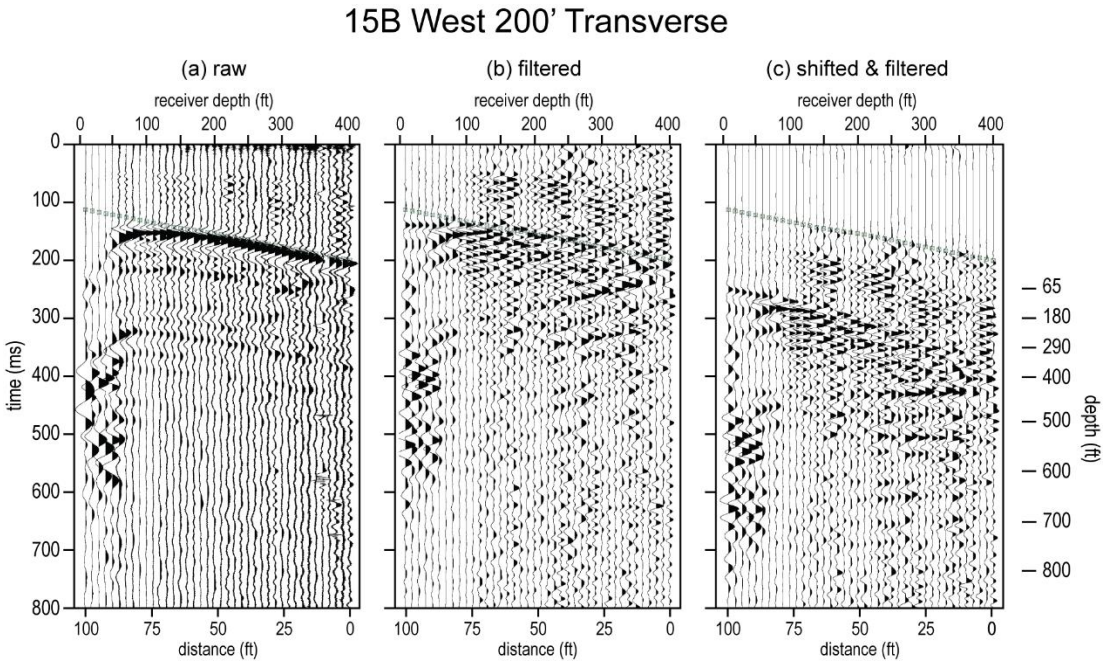

Figure A-15. Transverse VSP for the source station 200 ft west of Well 15B (*a*) unprocessed with picked first arrivals (green), (*b*) filtered, and (*c*) after static corrections, shifted to one-way vertically incident travel time.

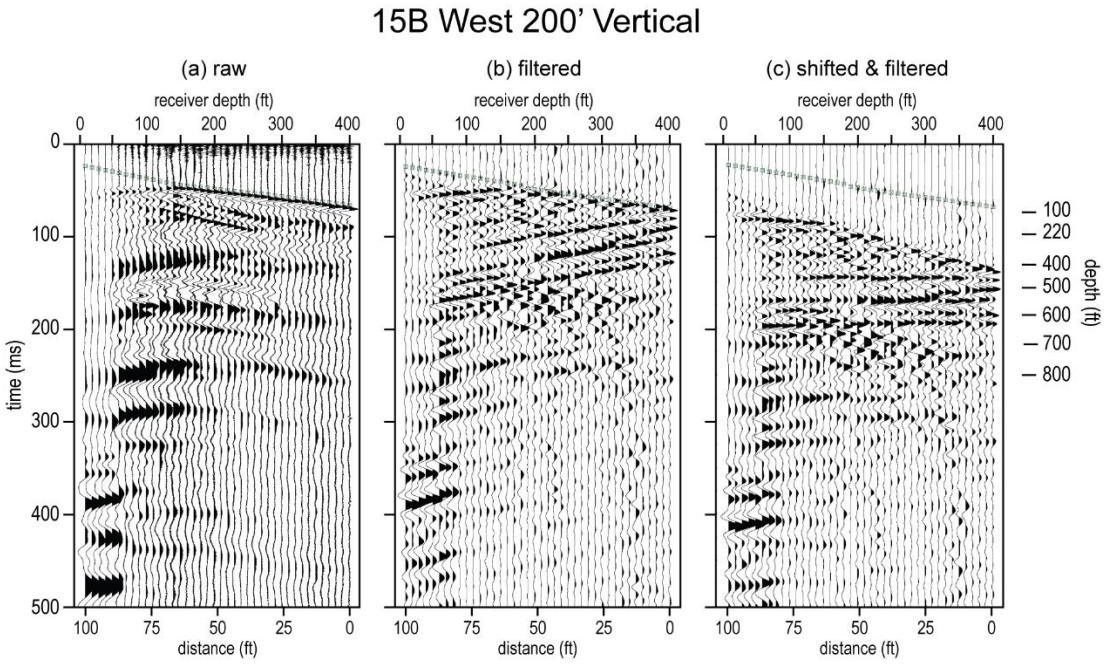

Figure A-16. Vertical VSP for the source station 200 ft west of Well 15B (*a*) unprocessed with picked first arrivals (green), (*b*) filtered, and (*c*) after static corrections, shifted to one-way vertically incident travel time.